JACS
JOURNAL OF THE AMERICAN CHEMICAL SOCIETY

Article

pubs.acs.org/JACS

Computation Sheds Insight into Iron Porphyrin Carbenes' Electronic Structure, Formation, and N−H Insertion Reactivity

Dina A. Sharon,[†] Dibyendu Mallick,[†] Binju Wang,[†] and Sason Shaik*[,†]

[†]Institute of Chemistry and The Lise Meitner-Minerva Center for Computational Quantum Chemistry, The Hebrew University of Jerusalem, 91904, Jerusalem, Israel

Supporting Information

ABSTRACT: Iron porphyrin carbenes constitute a new frontier of species with considerable synthetic potential. Exquisitely engineered myoglobin and cytochrome P450 enzymes can generate these complexes and facilitate the transformations they mediate. The current work harnesses density functional theoretical methods to provide insight into the electronic structure, formation, and N−H insertion reactivity of an iron porphyrin carbene, $[Fe(Por)(SCH_3)(CHCO_2Et)]^-$, a model of a complex believed to exist in an experimentally studied artificial metalloenzyme. The ground state electronic structure of the terminal form of this complex is an open-shell singlet, with two antiferromagnetically coupled electrons residing on the iron center and carbene ligand. *As we shall reveal, the bonding properties of* $[Fe(Por)(SCH_3)(CHCO_2Et)]^-$ *are remarkably analogous to those of ferric heme superoxide complexes.* The carbene forms by dinitrogen loss from ethyl diazoacetate. This reaction occurs preferentially through an open-shell singlet transition state: iron donates electron density to weaken the C−N bond undergoing cleavage. Once formed, the iron porphyrin carbene accomplishes N−H insertion via nucleophilic attack. The resulting ylide then rearranges, using an internal carbonyl base, to form an enol that leads to the product. The findings rationalize experimentally observed reactivity trends reported in artificial metalloenzymes employing iron porphyrin carbenes. Furthermore, these results suggest a possible expansion of enzymatic substrate scope, to include aliphatic amines. Thus, this work, among the first several computational explorations of these species, contributes insights and predictions to the surging interest in iron porphyrin carbenes and their synthetic potential.

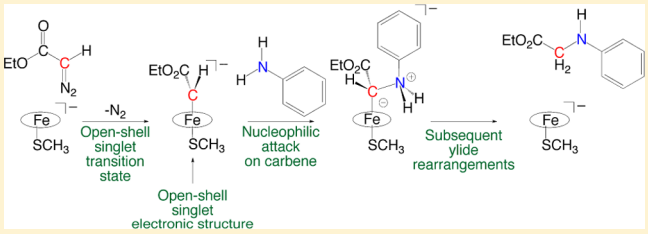

INTRODUCTION

Metallocarbenes occupy a prominent and growing position in synthetic chemists' toolboxes. Given the central role of carbon in organic molecules' scaffolds, a carbon-based reactive species, capable of forming bonds to other elements or other carbon atoms, represents a tantalizingly versatile synthetic building block. Metallocarbenes in general have the potential to play meaningful roles in the synthesis of a dazzling myriad of compounds, including pharmaceutically promising drugs, such as Thienamycin, Indatraline, and Maoecrystal V, accomplishing reactions such as N−H insertion, C−H insertion, and O−H insertion.[1−5] In metallocarbene work thus far, second- and third-row metals are prominent, though iron, a low-cost, abundant, and nontoxic alternative, has also demonstrated promise.[1]

Among iron carbenes, the structure and reactivity of iron porphyrin carbenes have captured chemists' interest. The pioneering report by Mansuy and colleagues of the first iron porphyrin carbene crystal structure facilitated understanding these complexes' structures and unlocked the door to future work.[6] Subsequent investigations obtained crystal structures and spectra of iron porphyrin carbenes with a variety of carbene substituents, axial ligands, and porphyrin substituents.[7−11] Iron porphyrin carbenes have been reported to mediate reactions including cyclopropanation,[12,13] N−H insertion,[14−20] C−H insertion,[21] carbonyl olefination,[22] and O−H insertion.[23] In addition to accomplishing many reactions, iron porphyrin carbenes can accomplish reactions under many different conditions: for instance, water-soluble iron porphyrins mediate cyclopropanation[13] and N−H insertion.[17,18]

Iron porphyrin carbene complexes rarely form in cytochrome P450 enzymes (P450s), and they often only appear over the course of drug metabolism.[24] Propelled by a drive to expand the reactivity of iron carbenes, Arnold, Fasan, Hauer, and their colleagues have studied and engineered P450 enzymes, as well as other heme enzymes, which host putative iron porphyrin carbenes.[25−32] These proposed species, with an iron−carbon bond, form by the reaction of the iron porphyrin with ethyl diazoacetate (EDA), whereby dinitrogen loss and iron−carbon bond formation are thought to generate the iron porphyrin carbene. Initial reports explored the ability of the proposed iron porphyrin carbenes to cyclopropanate alkenes (conceptually analogous to iron-oxo-mediated olefin epoxidation).[25,26] Subsequent work with artificial metalloenzymes revealed these putative iron porphyrin carbenes catalyze carbonyl olefination[31,32] and insert into amine N−H and thiol S−H bonds, to form C−N[28,29] and C−S[30] bonds, respectively. These reactions

Received: May 5, 2016
Published: June 27, 2016

DOI: 10.1021/jacs.6b04636
J. Am. Chem. Soc. 2016, 138, 9597−9610

Scheme 1. Formation and N−H Insertion Reactivity Pathway of a Model System of the Iron Porphyrin Carbene Studied by Arnold and Colleagues[28a]

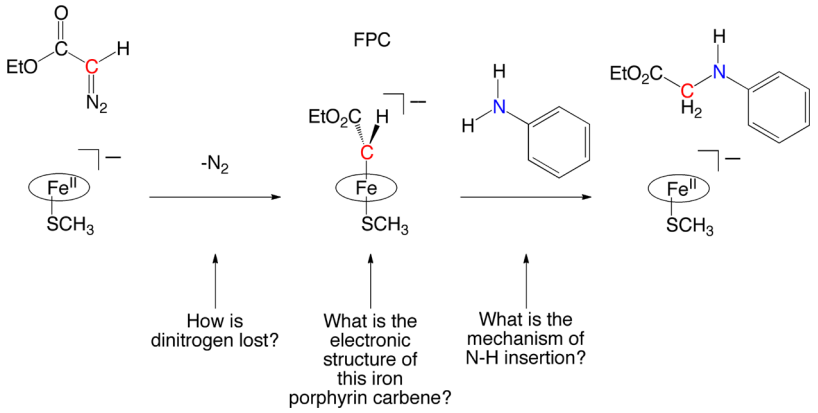

[a]The current work elucidates the electronic structure of this iron porphyrin carbene, as well as its formation and N−H insertion reactivity pathways. The oxidation state is not shown for the iron in the carbene complex, because that is an open question the current work will explore. The oval around iron represents the porphyrin ligand.

display a wide substrate scope and occur in high yields (some nearly quantitative) and with total turnover numbers in the hundreds or thousands. Arnold revealed, with competition experiments, that the proposed P450 iron porphyrin carbene preferentially accomplished N−H insertion, over alkene cyclopropanation.[28]

In light of the ability of artificial metalloenzymes to catalyze reactions effectively and with high stereoselectivity,[33−40] the pharmaceutical and synthetic prominence of C−N bonds,[41−43] and the ease with which this N−H insertion reaction occurs inside modified P450 enzymes,[28] studying the nature of the iron porphyrin carbene active species and the mechanism of iron porphyrin carbene formation and subsequent N−H insertion is of immense interest for both the chemical and enzymatic communities. Experimentalists have begun to investigate these questions, but much territory remains open for exploration. Though experimentalists have postulated the existence of the iron porphyrin carbene inside of modified cytochrome P450 and myoglobin enzymes, such complexes have only rarely been spectroscopically characterized inside wild type enzymes and involve carbenes quite different from that studied in this work.[44,45] To the best of our knowledge, an iron porphyrin carbene has never been spectroscopically characterized inside the artificial metalloenzymes where it has been proposed to catalyze reactions. Arnold and Fasan proposed that Fe(II) is the oxidation state of the iron porphyrin reacting with EDA.[25,26,28,29] Schematically, they depicted the iron in the carbene in the Fe(IV) oxidation state, but the evidence for such an assertion is not immediately apparent.[25,29]

Experimental work on enzymatic iron porphyrin carbene reactivity has not yet conclusively determined the N−H insertion mechanism. Experiments where oxygen and carbon monoxide, known to bind to iron, induce a decrease in the yield of the N−H insertion product confirmed iron's central role in this transformation.[28,29] Work by Fasan and colleagues on myoglobin-mediated S−H insertion, which may function similarly to N−H insertion, suggested an ylide intermediate may be present.[30] However, other reports on iron carbenes proposed they are capable of operating via radical mechanisms.[46] Woo and Gross have explored iron porphyrin carbene N−H insertion reactions in model systems, but given the Fe(III) oxidation state believed to be operative in their systems, this work, though insightful, may not be fully applicable to understanding enzymatic systems.[14,16]

Given the putative nature of the iron porphyrin carbene active species, and the lack of experimental structural detail on them and mechanistic detail on their reactivity and formation, computational work represents as an insightful key that can unlock insights about these complexes. By modeling different iron porphyrin carbene electronic structures and formation and reactivity pathways, computation can generate testable predictions that could contribute to developing a thorough mechanistic understanding. In turn, these insights can culminate in designing systems to improve upon existing ones, accomplishing the reaction faster, in higher yield, and with higher stereoselectivity.

Tatsumi and Hoffmann have reported the electronic structure of iron porphyrin carbenes,[47] focusing mostly on a pristine CH_2 carbene ligand. They elucidated the existence of five iron orbitals of different energies, in remarkable contrast to the orbital degeneracy observed in iron-oxo porphyrin complexes.[47−51] Despite this intriguing, early report, computational progress on iron porphyrin carbenes remained largely dormant for decades, with few findings of relevance to Arnold's system emerging.[52]

Recently, Zhang and co-workers investigated the electronic structure of a variety of iron porphyrin carbenes with either no axial ligand or a neutral *N*-methylimidazole axial ligand,[53] and they concluded that the most stable electronic state was a closed-shell singlet, with Fe(II) (not Fe(IV), as suggested by Arnold and Fasan).[25,29] This work substantiated the claim of iron porphyrin carbenes' existing as singlets by predicting spectroscopic parameters of the complexes in different spin states and comparing to experimental results.[7,8,54] Though a closed-shell singlet was explored, an open-shell singlet, as can be suggested by considering nonheme iron carbene systems,[55] was not studied. Building upon their electronic structure findings, Zhang and colleagues subsequently reported energy profiles for dinitrogen loss and carbene formation from a vast variety of iron porphyrin/diazo-containing carbene precursor systems, including one modeling Arnold's system. Zhang's group generalized its findings and concluded, without verifying, that all of the transition states for dinitrogen loss and the

DOI: 10.1021/jacs.6b04636
J. Am. Chem. Soc. 2016, 138, 9597−9610

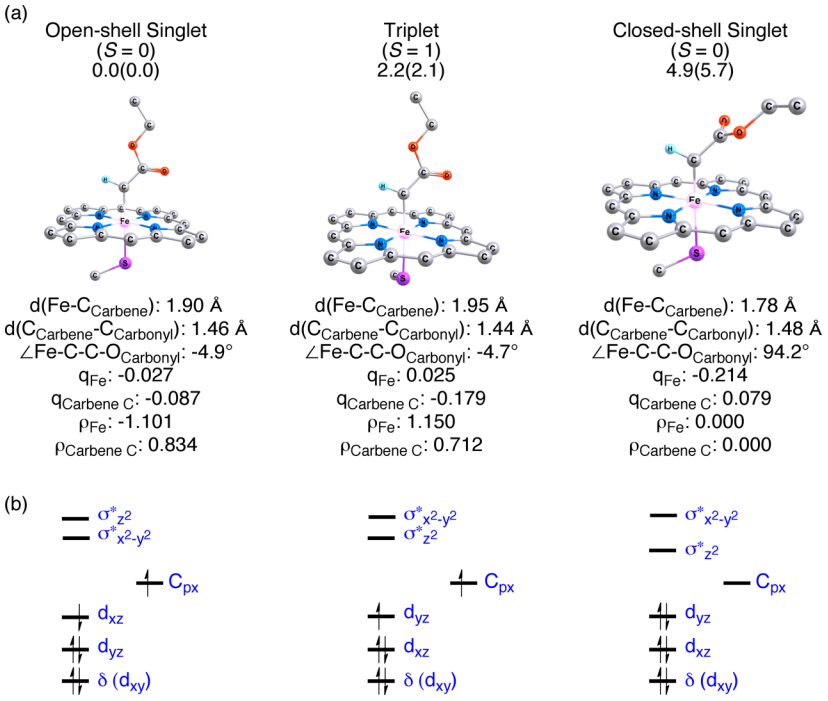

Figure 1. (a) Relative energies (in kcal/mol) of the lowest-lying electronic structures of the iron porphyrin carbene. Energies were computed at the B2//B1 level, and they are presented as relative electronic energy with zero-point correction outside of the parentheses and then relative Gibbs free energy inside the parentheses. Structures were optimized in chlorobenzene (SMD model). Values are dispersion-corrected. The structures, geometric parameters, NBO charges (q), and Mulliken spin densities (ρ) are also shown. For clarity, the only hydrogen atom shown is that bound to the carbene carbon. (b) The electronic structures of the open-shell singlet, the triplet, and the closed-shell singlet, respectively, determined from orbitals computed at the B2 level of theory.

resulting product iron porphyrin carbene complexes have closed-shell singlet ground states.[56]

Though computational reports on the electronic structure and formation of iron porphyrin carbenes exist, these have not yet explored electronic structure to the fullest extent possible. In contrast, to the best of our knowledge, nobody has yet harnessed computational techniques to investigate iron porphyrin carbenes' reactivity (in contrast to nonheme iron carbene systems, whose structure, formation, and reactivity have all been computationally studied[46,55,57,58]). Given this incomplete current understanding, we sought to more thoroughly study iron porphyrin carbenes' structure and formation. Subsequently, we investigated N−H insertion mediated by these species, in the first computational report of iron porphyrin carbene reactivity. Scheme 1 presents the system of interest, $[Fe(Por)(SCH_3)(CHCO_2Et)]^-$ (FPC), and it introduces questions that this work explores about the system. Given this flourishing experimental state of affairs, and considering the paucity of computational work on iron porphyrin carbenes, alongside the rich computational literature on iron-oxo complexes,[59,60] the need for further computational exploration resonates strongly. As we shall demonstrate, the iron porphyrin carbene's ground state is an open-shell singlet, analogous to that of ferric superoxide porphyrin complexes.[61−63] The barrier for dinitrogen loss from EDA to form the carbene is the lowest on the open-shell singlet surface. The N−H insertion product forms from the amine's nucleophilic attack on the carbene carbon and the resulting ylide's subsequent rearrangement through a five-membered ring transition state. This work represents a significant and novel step into an intriguing new reactivity frontier, unlocking the immense potential of iron porphyrin carbenes by exploring their structure and their formation and N−H insertion reactivity pathways.

COMPUTATIONAL METHODS

All structures were optimized using the Gaussian 09 software program,[64] employing the UB3LYP functional,[65−68] with the LANL2DZ basis set with an effective core potential for iron[69−71] and the 6-31G(d) basis set[72−75] for all other atoms. Collectively, this combination of LANL2DZ and 6-31G(d) will subsequently be referred to as B1. Optimizations were performed in chlorobenzene solvent, using the SMD solvation model.[76] This solvent was selected to mimic the nonpolar protein environment, following the precedent established by previous studies exploring enzymatic reactions in model systems.[48,77,78] With the optimized geometries, single-point energy calculations in chlorobenzene solvent were performed using the all-electron Def2-TZVP basis set for all atoms.[79,80] Dispersion corrections were computed with Grimme's D3 method.[81] Natural Bond Orbital (NBO) analysis provided Natural Population Analysis (NPA) charges.[82]

After optimization, frequency analyses were performed at the B1 level for all species in order to characterize the nature of the stationary points. The zero-point energy and thermal correction to Gibbs free energy obtained from the B1 frequency analysis were added to the B2 single-point energies. In addition, guess structures of several species, input into optimization, were based on previously published work.[56] Whenever possible, intrinsic reaction coordinate (IRC) calculations were performed to connect the transition states with their corresponding reactants and products.

Though previous work on iron porphyrin carbenes employed functionals other than UB3LYP, this past work selected which functional to use based on geometric benchmarking analyses and some very rough energetic benchmarking.[53,56] Given our group's extensive experience with iron-oxo chemistry, and our and others' findings that UB3LYP is an accurate functional in studying such systems,[59,83−85] we chose to apply UB3LYP to our studies of iron porphyrin carbenes. We

DOI: 10.1021/jacs.6b04636
J. Am. Chem. Soc. 2016, 138, 9597−9610

have also tested other functionals, namely the UM06-L,[86] UTPSSh,[87] UM06,[88] and UBMK[89] functionals, in order to verify the robustness of conclusions obtained with UB3LYP. Table S1 presents energy gaps between different electronic structures obtained with these functionals.

For all species, the electronic structure was checked by visualizing spin-natural orbitals (SNOs) (and often also Kohn−Sham natural orbitals (NOs)) at the B1 level and spin-natural orbitals at the B2 level. In addition, Kohn−Sham corresponding orbitals (KSCOs) were visualized to better understand the open-shell singlet's electronic structure. Resolutions of orbitals presented herein were selected on the basis of each individual orbital, to best capture its bonding features. In order to obtain the open-shell singlet electronic structure, a "stable = opt" calculation[90−92] was performed on a guessed geometry for the desired species, followed by a geometry optimization with this guess. The "guess = alter" keyword was sometimes employed to obtain different open-shell singlet electronic structures.

Though there have been some uncertainties about the role DFT can play in understanding open-shell singlets,[93,94] Abe, Schreiner, and colleagues have recently demonstrated it is an insightful technique for studying such systems.[95−97] Abe advised use of a Yamaguchi correction[98] for open-shell singlets, which could not be implemented here given the high $\langle S^2 \rangle$ values after spin annihilation, as Table S2 presents, and the differences in singlet and triplet electronic structure, as will be explained in the Results and Discussion. If used, this correction should lower the energy of the open-shell singlet, already the lowest-energy species. Table S2 shows the energy changes upon Yamaguchi correction[99] for open-shell singlet species reported in this text. The correction generally stabilizes open-shell singlets, but the annihilation of the spin contaminant is incomplete in the species in the current work. Whether or not a Yamaguchi correction is employed, iron porphyrin carbenes constitute physical states similar to biradicaloids, which generally exhibit OSS states alongside triplet and CSS states.

The porphyrin ligand was modeled as porphine, as has been done in similar model system studies.[78,85] Interestingly, Arnold and colleagues found an iron porphyrin outside of the enzyme could mediate N−H insertion, and this result helps to justify the use of a model system to gain insight into the enzyme's active site.[28] The cysteine ligand was modeled as SCH_3, as has been done in previous model system studies[100] (cysteine was modeled given Arnold's finding that it gave rise to the highest N−H insertion reactivity[28]). We also tested the SH ligand. The results are similar to those obtained with the SCH_3 ligand, as shown in Tables S3−S6. The carbene used was $CHCO_2Et$, as used in most experimental work.[28]

RESULTS AND DISCUSSION

1. Iron Porphyrin Carbene Electronic Structure.

1.1. Geometric and Electronic Structure. Figure 1a presents the relative energies, geometries, and key structural parameters of the three lowest-energy electronic structures of $[Fe(Por)(SCH_3)(CHCO_2Et)]^-$. The open-shell singlet (OSS) is the ground state, the triplet is the next highest in energy, and the closed-shell singlet (CSS) is the highest in energy of the three states. Having the triplet be lower in energy than the CSS is a typical situation for species with a singlet diradicaloid ground state. We also tested other functionals (Table S1), and the UTPSSh, UM06, and UBMK functionals gave rise to a relative ordering of the spin states identical to that obtained with UB3LYP, confirming the conclusion's robustness.

Looking at the three species, the pair with the most similar Fe−C distances and Fe−C−C−O dihedral angles is the OSS and the triplet. While the Fe−C distances for the OSS and the triplet are 1.90 and 1.95 Å, respectively, the Fe−C distance for the CSS is 1.78 Å. The Fe−C−C−O dihedral angle in the CSS is twisted approximately 90° compared to the OSS and triplet. The observation of more drastic differences between the OSS and CSS, with the same overall spin, and less drastic differences between the OSS and the triplet, instigates further investigation of the electronic structures of these species.

Given Arnold, Fasan, and colleagues' thorough proof of a reduced iron porphyrin carbene as the active species,[25,26,28,29] possible electronic structures of this complex must render the complex monoanionic overall. With a dianionic porphyrin ring and a monoanionic cysteine ligand (abbreviated here as SCH_3^-), there must be an overall +2 charge on the iron and carbene components when grouped together. One way to achieve this distribution is to have Fe(III) (with a d^5 configuration) and a carbene radical (formally a carbene anion radical), as occurs for the open-shell singlet and triplet. Figure 1b presents these electronic structures on the left (OSS) and in the middle (triplet). The open-shell singlet exhibits antiferromagnetic coupling between the carbene carbon-centered radical and the unpaired d-electron on the iron atom. Meanwhile, the triplet exhibits ferromagnetic coupling. The spin densities in Figure 1a bolster the claims of ferromagnetic and antiferromagnetic coupling and significant localization of spin on iron and the carbene carbon. A second feasible charge distribution is to have Fe(II) (with a d^6 configuration) and a carbene without any unpaired electrons, as occurs for the CSS, shown on the right-hand side of Figure 1b. The NBO charges in Figure 1a support the claim iron is more oxidized (and the carbene is more reduced) in the OSS and the triplet than in the CSS. The subsequent sections will explore the orbital occupancies and nature of bonding in these three species.

1.2. The Open-Shell Singlet: Bonding and Orbital Considerations. To form the iron porphyrin carbene, the $[Fe(Por)(SCH_3)]^-$ and the $CHCO_2Et$ fragments' orbitals must interact. Figure 2 presents a schematic orbital interaction diagram (see Figure S1 for a more detailed diagram). An sp^2 carbene orbital which has one lobe oriented toward the iron donates its electron pair to the vacant d_{z^2} orbital of iron to form an Fe−C σ bond in the iron porphyrin carbene. In addition, the doubly occupied d_{xz} orbital, with π symmetry, can mix weakly with a vacant carbene p_x-orbital, to form a slightly bonding and antibonding combination. One of these two orbitals is mostly on iron, so much so that it is called here d_{xz}. The other orbital is mostly on carbon, so much so that we chose to name it C_{px}. The other iron d-orbital of π symmetry cannot mix with any carbene orbital, so it is nonbonding and is called d_{yz}.

In the OSS, the spin-natural orbitals (SNOs) consist of C_{px}, with an occupancy of 0.88, and d_{xz}, with an occupancy of −0.88, as Figure 3a depicts. This nonunity occupancy indicates that the two SNOs are mutually interacting. Thus, the OSS has an α-electron and a β-electron that are neither perfectly isolated from each other (SNO occupancies are not 1.00), nor bonded strongly. The interacting nature of the SNOs is reflected in the population of the complex's natural orbitals (NOs) in Figure 3b, which show Fe−C bonding and antibonding interactions. Resolving them to Kohn−Sham corresponding orbitals (KSCOs) in Figure 3c clarifies the situation. The KSCOs are more localized on the two atoms than the NOs, suggesting the two electrons have some degree of separation. As de Bruin's cobalt and iridium carbene studies discuss,[101,102] from a technical perspective, FPC can be thought of as an iron-bound carbene radical, as opposed to a traditional metal carbene. However, for consistency with prior work and clarity, though this caveat is noted, we retain the term "iron porphyrin carbene" in the current work.

DOI: 10.1021/jacs.6b04636
J. Am. Chem. Soc. 2016, 138, 9597−9610

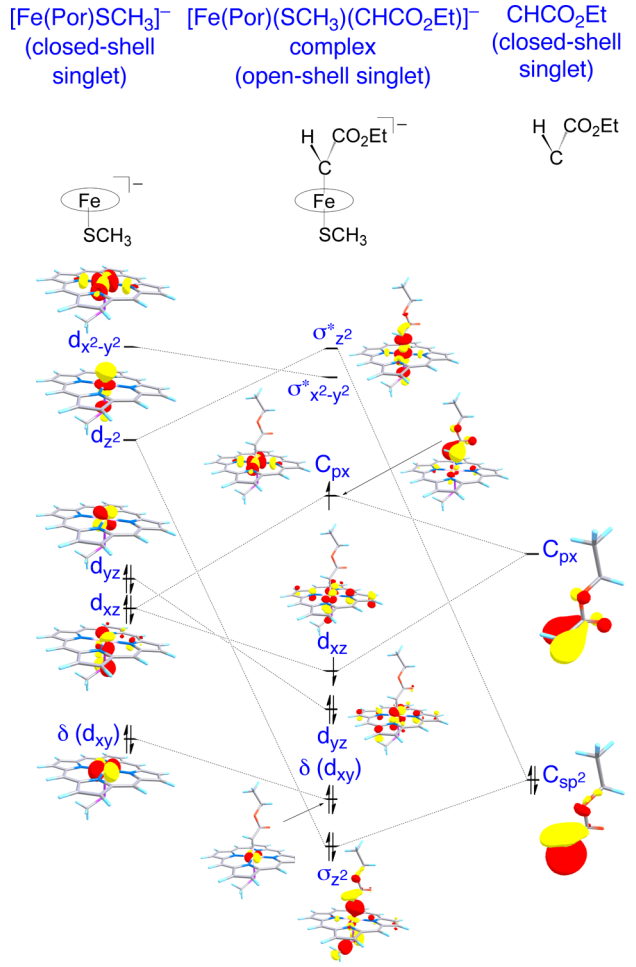

Figure 2. Schematic molecular orbital interaction diagram for FPC in its lowest-energy open-shell singlet state, considering it being built from the fragments $[Fe(Por)(SCH_3)]^-$ (left) and $CHCO_2Et$ (right). Orbitals were generated at the B2 level from single point calculations.

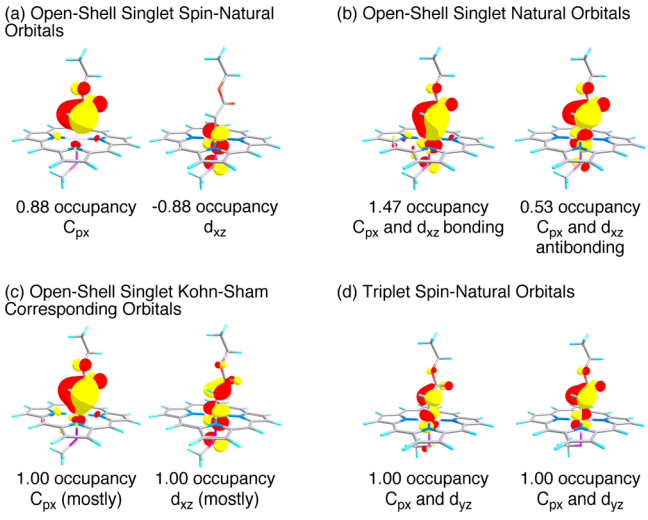

Figure 3. Spin-natural orbitals (a), natural orbitals (b), and Kohn–Sham corresponding orbitals (c) of the open-shell singlet and the spin-natural orbitals of the triplet (d). All orbitals were computed at the B2 level of theory and are shown along with their occupancies.

1.3. Similarities to Superoxide Complexes and Comparisons to Previous Iron Porphyrin Carbene Work. A close examination of the orbital interaction diagram and nature of the molecular orbitals of the iron porphyrin carbene complex reveals a striking similarity between the electronic structural features of FPC and iron(III) porphyrin superoxide complexes, and this analogy opens up a new dimension of iron carbene chemistry. Heme superoxide complexes also originate from Fe(II) and a neutral ligand (O_2). In both systems, electron donation from the ligand to the iron d_{z^2} orbital forms a σ bond between iron and the ligand. The iron center donates electron density to the dioxygen moiety, in order to create Fe(III) and a superoxide radical,[61−63] a structure originally proposed by Weiss.[103] This is similar to the iron's donating electron density to the carbene to form Fe(III) and a carbene radical (formally a carbene anion radical). The lowest-energy state of ferric superoxide complexes is an open-shell singlet, with antiferromagnetic coupling between the electrons on the iron and the superoxide radical, as our group and that of Parrinello have demonstrated.[61,62] An iron d-orbital of π symmetry and the oxygen O−O π^* orbital engage in this coupling, similar to the d_{xz} and carbene C_{px} interacting in the case of the iron porphyrin carbene, as the orbital diagrams that Scheme 2 compares depict.[61,62] As was described for the ferric superoxide species, in the iron porphyrin carbene, the antiferromagnetically coupled electrons exhibit a weak bonding interaction, but not a formal full bond.[61,62] Promisingly, our group previously found, for ferric superoxide species, that DFT gave results similar to those of complete active space self-consistent field (CASSCF) techniques, confirming the appropriateness of DFT for describing heme iron OSS systems.[61]

We note that Zhang and colleagues initially studied several iron porphyrin carbenes, for which the closed-shell singlet was found to be the ground state.[53] Then, in subsequent work, they assumed they could generalize this electronic structure finding to other iron porphyrin carbenes complexes,[56] including $[Fe(Por)(SH)(CHCO_2Et)]^-$, identical to that used in the current work except for the axial ligand. Such a generalization overlooked the intriguing differences in electronic structure that the carbene ligand and axial ligand can trigger. Hence, the work did not report the OSS and triplet species that are lower in energy than the reported CSS. Analyzing Zhang's structure, with the exact methods used by his group, reveals a lower-energy electronic structure than he reported: at the single-point level (with the optimized CSS geometry), the OSS is 4.3 kcal/mol lower in electronic energy than the CSS. Table S7 and Figure S8 present this result, confirming that Zhang and colleagues overlooked this crucial electronic structure. Furthermore, optimizing this OSS would likely yield an even lower energy.

Chirik, DeBeer, and colleagues' work on a nonheme iron carbene system with antiferromagnetic coupling,[55] as well as work on nonheme cobalt carbenes,[104] provide a further precedent for our claim of antiferromagnetic coupling between iron and the carbene, in contrast to Zhang and colleagues' report. Furthermore, the claim of a C_{px} radical finds precedent in de Bruin and others' work on cobalt porphyrin carbenes,[101,105,106] as well as work on oxidized iron porphyrin carbenes[107] and other systems.[102,108−110] Table S8 and Figure S9 reveal the CSS is not the most stable electronic structure with a $CHCO_2Et$ carbene and a model of a histidine or serine axial ligand (the OSS is lower-energy for these complexes): these preliminary findings highlight that exploring the range of iron porphyrin carbenes with an OSS ground state is an intriguing avenue for future work.

DOI: 10.1021/jacs.6b04636
J. Am. Chem. Soc. 2016, 138, 9597−9610

Scheme 2. Orbital Diagrams for $[Fe(Por)(SCH_3)(CHCO_2Et)]^-$ (Left) and a Ferric Superoxide Complex (Right)[a]

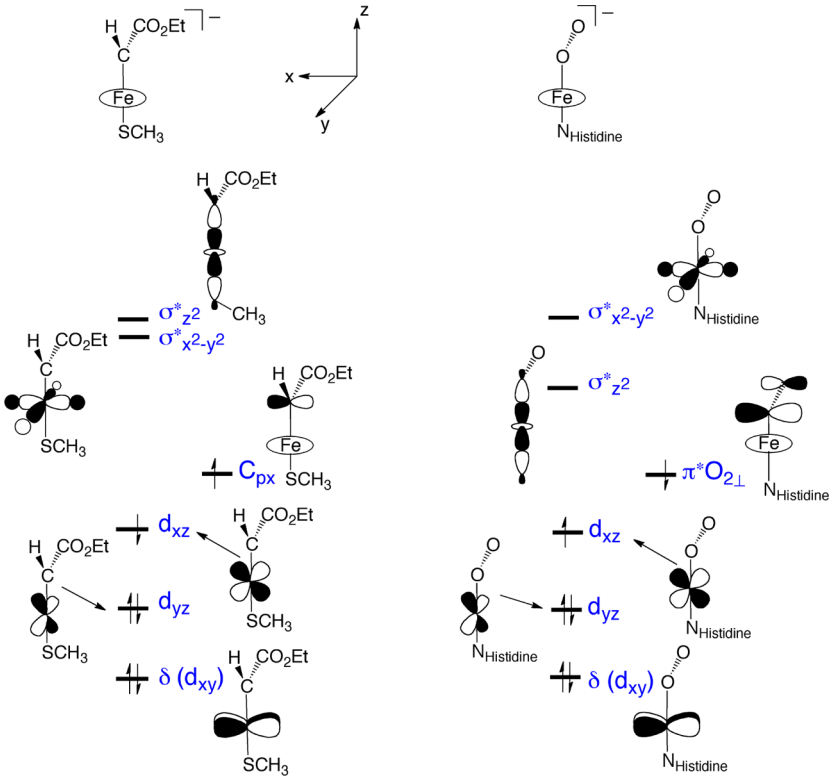

[a]The diagram on the right was adapted from work of the Jerusalem group on myoglobin, and N_{His} represents the histidine ligand in this myoglobin system.[61]

1.4. Alternative Electronic Structures. To return to this work's system, the CSS FPC species, when optimized, does not yield a stable wave function: the OSS wave function is lower in energy (see Table S9 and Figure S10). The CSS is an excited singlet state. Figure 3a shows the electron on the C_{px} orbital can be delocalized onto the adjacent carbonyl moiety in the OSS. This delocalization outweighs the stabilization that would come from this electron's residing on iron, forming a CSS. Why can iron not be further oxidized, forming Fe(IV)? All efforts to obtain this electronic structure failed, as previously reported.[53] This situation likely arose because the carbene lacks the two perpendicular p(π)-type orbitals to interact with the d_{xz}/d_{yz} orbitals and generate the two π and two π^* orbitals which typify Fe(IV)═O units. However, by enabling electron delocalization, the CO_2Et carbonyl group helps the carbene accept electron density.[105] Hence, an Fe(III)-superoxo type electronic structure arises. Tuning carbene substituents may facilitate altering the complex's ground state.

The other low-lying electronic state, the triplet, differs from the OSS by more than a simple spin flip (see Figure 1). Figure 3d presents the triplet's SNOs. Here, d_{yz} and C_{px} are singly occupied, unlike in the OSS, where d_{xz} and C_{px} are singly occupied. It should be noted both d_{yz} and C_{px} appear in both SNOs in Figure 3d. In the OSS, the ground state has two electrons with opposite spins placed in parallel orbitals: this is stabilizing because they antiferromagnetically couple. Meanwhile, in the triplet, the electrons' spins are oriented identically. Thus, the two electrons reside in orbitals oriented perpendicularly to each other, minimizing the repulsion between identically oriented spins centered on different atoms. An alternate OSS electronic structure, with d_{yz} and C_{px} singly occupied, is 6.9 kcal/mol higher in energy than the ground state OSS electronic structure at the B1 level (see Figure S11), further validating the claim antiferromagnetic coupling between electrons in orbitals oriented parallel to each other stabilizes the ground state OSS electronic structure. These insights into electronic structure facilitate interpreting the different spin states' geometries in Figure 1. While the OSS antiferromagnetic coupling is not formally a bond, it is a stabilizing interaction and draws the Fe and C closer than in the triplet. The OSS and triplet have $Fe-C_{Carbene}-C_{Carbonyl}-O_{Carbonyl}$ dihedral angles near zero, so the electron on the carbene radical can be delocalized onto the adjacent carbonyl group.

We also strove to understand the structure of the one-electron oxidized species, $[Fe(Por)(SCH_3)(CHCO_2Et)]$, which has also been proposed as an intermediate in carbene-mediated reactions in model systems.[14] First, we considered the terminal carbene species. As Figure S12 presents, the lowest-energy state of $[Fe(Por)(SCH_3)(CHCO_2Et)]$ is a doublet with antiferromagnetic coupling between iron's d_{xz} and carbon's C_{px} orbitals (analogous to the coupling found in the one-electron reduced form). Indeed, the SNOs in Figure S13 reveal the lowest-energy doublet differs from the OSS state of the reduced carbene complex only by the removal of one electron from the a_{2u}/S orbital. Similarly, both the quartet (oxidized) and triplet (reduced) species exhibit ferromagnetic coupling, with a singly occupied d_{yz}, and the oxidized quartet state also has one electron removed from the a_{2u}/S orbital, compared to the reduced triplet state. In the lowest-energy doublet, the unpaired electron on iron has β spin, so it can couple antiferromagnetically with both the a_{2u}/S and C_{px} electrons. These findings agree with previous work claiming there is some amount of spin

DOI: 10.1021/jacs.6b04636
J. Am. Chem. Soc. 2016, 138, 9597−9610

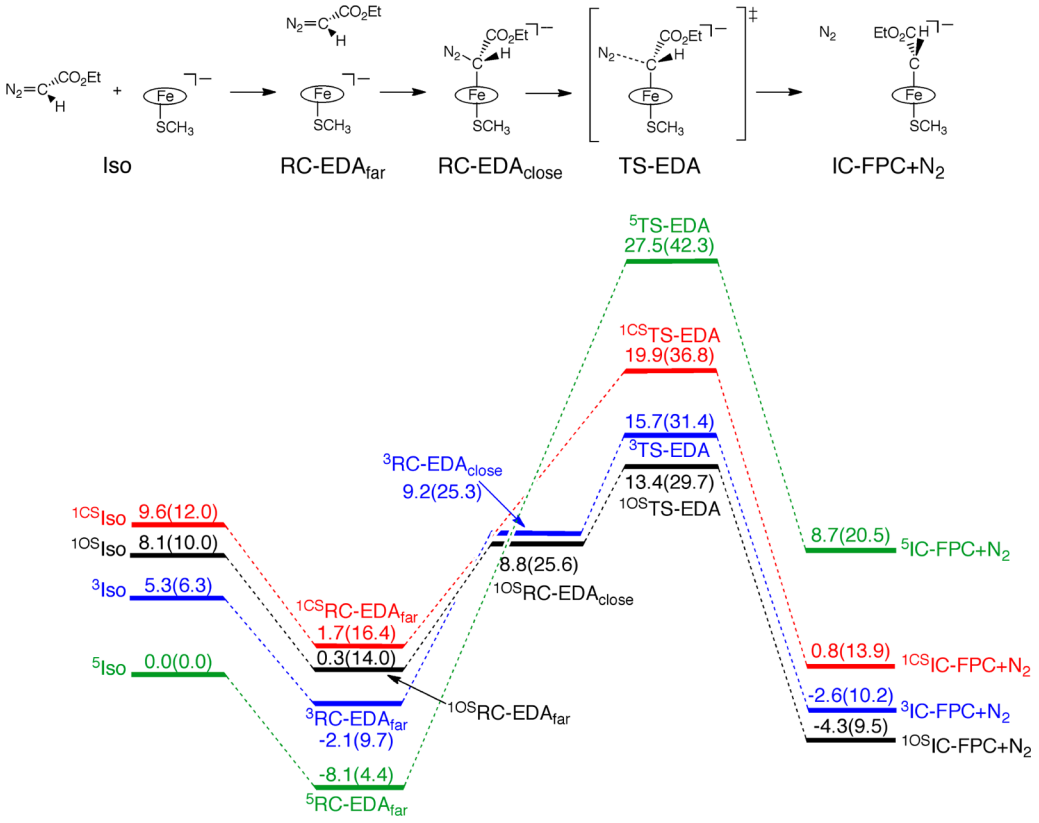

Figure 4. Energy profile for dinitrogen loss from EDA to form the iron porphyrin carbene species. Energies were computed at the B2//B1 level, and they are presented as relative electronic energy with zero-point correction outside of the parentheses and then relative Gibbs free energy inside the parentheses. Structures were optimized in chlorobenzene (SMD model). All values are dispersion-corrected. Note that this profile is plotted with respect to the electronic energies with zero-point correction.

density on the carbene moiety in terminal oxidized iron porphyrin carbenes.[107]

Experimental[9,10] and computational[107] studies suggest the oxidized carbene complex may exist in a bridged form (carbon bridging iron and a porphyrin meso nitrogen). Preliminary results (Figure S15) show not only that the bridged oxidized carbene is over 20 kcal/mol more stable than the terminal carbene but also that the barrier to form the bridged species from the terminal species is quite low. Further investigation of this bridged structure of the oxidized carbene and possible subsequent transformations it has been proposed to undergo[9,10] is of high interest.

We have investigated the bridged structure for the reduced form as well (Figure S17): though it is thermodynamically feasible, we found its formation from the terminal species to have a higher barrier than the barrier for the oxidized form. Indeed, experimental work has proposed the reduced carbene is terminal and the oxidized carbene is bridged.[9] The subsequent section discusses, for the reduced species, how the terminal carbene is the initial carbene formation reaction product (using intrinsic reaction coordinate calculations). The bridging barrier is higher than the barrier for terminal carbene reactivity from the reactant complex reported later in the manuscript. Also, previous cobalt porphyrin carbene work found the bridged species not to be reactive, so even if the bridged species formed, it is likely it would not be of interest for this reactivity study.[101] Thus, we did not consider the reduced bridged species further in this work, though it may be of interest in future studies.

2. Iron Porphyrin Carbene Formation. *2.1. Reactivity Scheme.* Now that we have explored FPC's electronic structure, we can harness these insights in order to understand its formation and reactivity. In this work, ethyl diazoacetate (EDA) is studied because experimental work often uses it.[28,29] Dinitrogen loss from EDA to form the iron porphyrin carbene constitutes the most feasible N_2 loss pathway. Figure 4 presents the energy profile for this process. An alternative amine-assisted N_2 loss pathway, postulated by Gross and colleagues[16] in a more oxidized iron system, was also considered. However, energy scans did not yield the desired transition state. Furthermore, the more electron-rich reduced iron porphyrin studied should be able to better, on its own, promote N_2 loss from EDA to yield FPC than Gross' oxidized species can.

Initially, in the separated reactants, iron's ground state is a quintet. Subsequently, in the RC-EDA$_{far}$, the quintet remains the lowest-energy state (RC-EDA$_{far}$ represents the reactant complex with iron and EDA far from each other, with Fe−$C_{Carbene\ C\ precursor}$ distances over 3.50 Å and without any meaningful Fe-EDA interaction). Two spin states, the OSS and the triplet, have an additional, higher-energy reactant complex, RC-EDA$_{close}$, with a meaningful EDA carbon−iron interaction (e.g., there was a 2.23 Å Fe−$C_{Carbene\ C\ precursor}$ distance in ^{1OS}RC-EDA$_{close}$). IRC calculations from ^{1OS}TS-EDA and ^{3}TS-EDA yielded the RC-EDA$_{close}$ species, whereas IRC calculations from ^{1CS}TS-EDA and ^{5}TS-EDA yielded the RC-EDA$_{far}$ species. The ^{1OS}RC-EDA$_{far}$ and ^{3}RC-EDA$_{far}$ species were then obtained, in order to better understand the spin states' ordering. Attempts to optimize ^{1CS}RC-EDA$_{close}$ and ^{5}RC-EDA$_{close}$ did not yield species with meaningful Fe−C bonds or reasonable energies.

DOI: 10.1021/jacs.6b04636
J. Am. Chem. Soc. 2016, 138, 9597−9610

^{1OS}TS-EDA is the lowest-energy transition state, with a Gibbs free energy barrier of 29.7 kcal/mol. This is 1.7 and 7.1 kcal/mol lower in energy than ^{3}TS-EDA and ^{1CS}TS-EDA, respectively. Zhang and colleagues studied the N_2 loss process for a very similar system, with EDA and $[Fe(Por)(SH)]^-$. They only considered the CSS transition state for this process. With the ωB97XD functional, they found the Gibbs free energy barrier from the isolated quintet iron porphyrin and EDA to the CSS N_2 loss transition state to be 37.0 kcal/mol.[56] The present UB3LYP work found the Gibbs free energy barrier from the isolated quintet $[Fe(Por)(SCH_3)]^-$ and singlet EDA reactants to ^{1CS}TS-EDA is 36.8 kcal/mol. This match confirms that results from the two studies can be compared. This comparison reveals Zhang and colleagues may have missed the significantly lower-energy transition states, ^{1OS}TS-EDA and ^{3}TS-EDA.

This barrier of 29.7 kcal/mol represents a significant improvement upon the previously reported parameter, but is still a high barrier: several rationales have been proposed.[56] First, as Zhang noted,[56] these experiments' low enzyme loadings lead to large amounts of EDA relative to the enzyme and favor RC formation in the enzyme.[25,28] The barrier from the isolated reactants overestimates the entropy involved if the reaction starts from a reactant complex in the enzyme system: indeed, the Gibbs free energy barrier from ^{5}RC-EDA$_{far}$ has a lower value, 25.3 kcal/mol. Second, the enzyme environment may lower the barrier from the reactant complex to the transition state, below the value computed here:[56] Arnold, Fasan, and colleagues meticulously sculpted their enzymes by introducing mutations,[25,26,28,29] which can perhaps alleviate the energetic penalty of N_2 loss. In summary, the enzymatic environment may lower the reaction barrier by decreasing the entropic contribution to the barrier or stabilizing the transition state. The enzyme can bring the reactants close to each other, to form a reactant complex. Relative to this enzymatic reactant complex, the loss of entropy in the transition state is less severe as compared to the loss of entropy relative to the isolated reactants (as could be the case in a model system). Indeed, N−H insertion using an iron porphyrin model system occurred less effectively than enzymatic N−H insertion, suggesting the enzyme lowers the barrier for at least one reaction step.[29] The current work's model system does not capture the protein's contribution. Holistically studying protein effects with quantum mechanical/molecular mechanical techniques represents a promising avenue for further work. The barrier associated with the computed ^{1OS}TS-EDA is much lower in energy than Zhang's CSS barrier, and the enzymatic barriers may be lower than the computed values.

2.2. Insights into Electronic Structure. Why is the OSS the lowest-energy N_2 loss transition state? The SNOs of ^{1OS}RC-EDA$_{close}$ reveal that iron donates electron density to EDA (Figure 5a). Recent reports similarly found spin density on the N_2 moiety of rhodium and copper alkyl diazoacetate systems.[110,111] This interaction leads to a significant Fe−C bond, of 2.23 Å. This electron donated from iron to EDA enters a C−N antibonding orbital, resulting in a significantly longer C−N distance in ^{1OS}RC-EDA$_{close}$ than in ^{1CS}RC-EDA$_{far}$ (Table S11). NBO analysis confirms electron donation occurs on the OSS surface but not the CSS surface: while EDA has an NBO charge of 0.014 in ^{1CS}RC-EDA$_{far}$, it has an NBO charge of −0.471 in ^{1OS}RC-EDA$_{close}$. This situation is reminiscent of iron-oxo porphyrin formation, in how electron donation from iron facilitates forming the active species.[59,112]

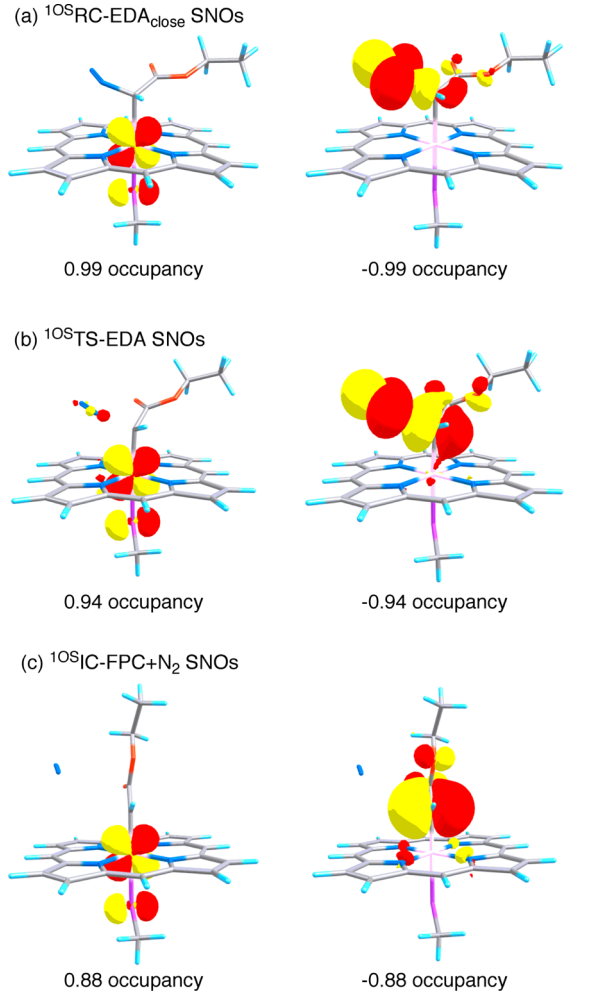

Figure 5. Spin-natural orbitals of the open-shell singlet RC, TS, and IC for the iron porphyrin carbene's formation. All orbitals were computed at the B2 level of theory and are shown along with their occupancies.

Electron donation is a one-electron process, not a two-electron process, and this fact explains why electron transfer does not occur on the CSS surface. In order for an electron to be transferred from iron to the EDA/forming N_2 moiety, the electron must either initially be unpaired (reside in a singly occupied orbital) or become unpaired over the course of the reaction (migrate from a doubly occupied orbital, leaving a singly occupied electron in this orbital). The electron migrates to an empty orbital, resulting in an unpaired electron residing on the EDA/forming N_2 moiety. On the CSS surface, this transfer of a single electron cannot occur, because a CSS, by definition, does not have any unpaired electrons.

The SNOs of ^{1OS}TS-EDA (Figure 5b) show electron donation from iron to carbon progresses during the reaction. Going from ^{1OS}RC-EDA to ^{1OS}TS-EDA, the EDA SNO involves visibly more contribution from carbon in ^{1OS}TS-EDA. The population of the C−N antibonding orbital in the OSS likely helps to cleave the C−N bond and lower the barrier for N_2 loss relative to the CSS barrier. Then, the SNOs of the carbene product resulting from ^{1OS}TS-EDA (Figure 5c) show that, at the culmination of the reaction, ^{1OS}FPC is formed. The N_2 on EDA provides an opportunity for electron donation from iron to EDA in ^{1OS}RC-EDA$_{close}$, stabilizing ^{1OS}TS-EDA and leading to formation of a carbene radical in ^{1OS}IC-FPC+N_2

DOI: 10.1021/jacs.6b04636
J. Am. Chem. Soc. 2016, 138, 9597−9610

Scheme 3. Mechanistic Possibilities for N−H Insertion Mediated by FPC

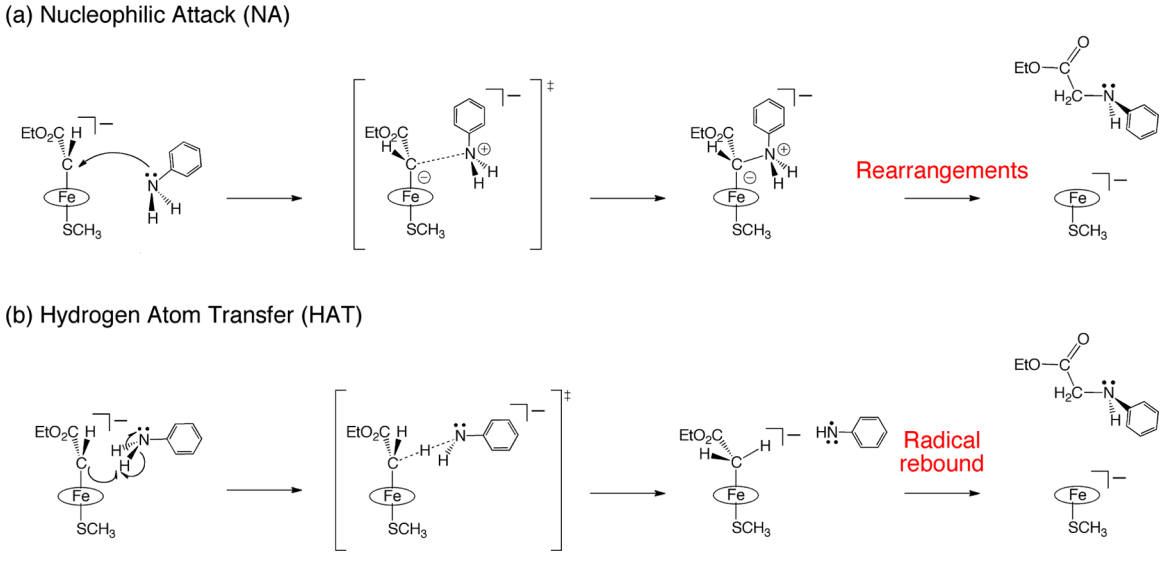

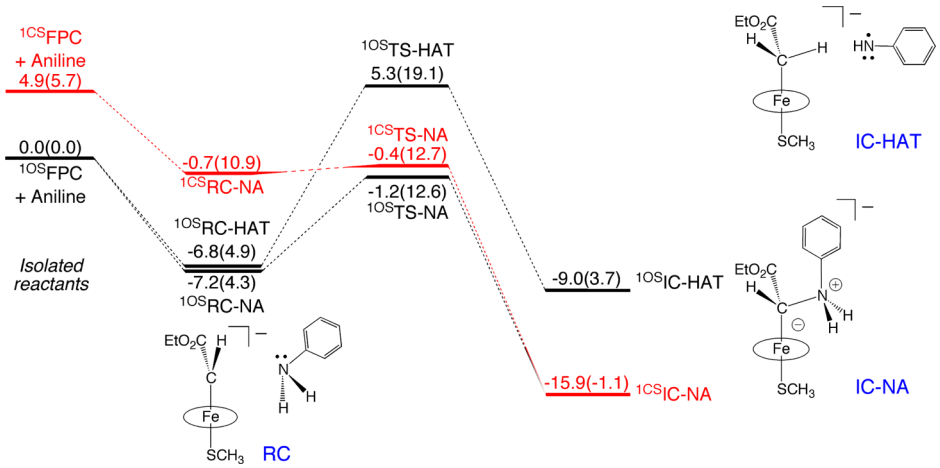

Figure 6. Energy profile for nucleophilic attack (NA) of aniline on the iron porphyrin carbene and hydrogen atom transfer (HAT) from aniline to the carbene. Nucleophilic attack was studied on the CSS and OSS surfaces, and HAT was studied on the OSS surface. Energies were computed at the B2//B1 level, and they are presented as relative electronic energy with zero-point correction outside of the parentheses and then relative Gibbs free energy inside the parentheses. Structures were optimized in chlorobenzene (SMD model). All values are dispersion-corrected. Note that this profile is plotted with respect to the electronic energies with zero-point correction.

(intermediate complex). Having explored FPC's electronic structure and formation, its reactivity beckons investigation.

3. Iron Porphyrin Carbene N−H Insertion Reactivity. *3.1. First Step: Nucleophilic Attack or Hydrogen Atom Transfer?* Aniline was the substrate in this study, given the use of it and its derivatives in experimental work.[28,29] Surveying the literature and this work's findings, two major mechanistic possibilities for N−H insertion emerge. First, previous studies on this reaction (and the related S−H insertion process) have suggested it follows a nucleophilic attack pathway, yielding an ylide intermediate.[14,17,30] Fasan and colleagues even observed evidence of an ylide by using a diagnostic substrate.[30] Scheme 3a presents this postulated mechanism. This ylide would then rearrange (by proton transfers and dissociation from iron) to yield the alkylated amine.

The second possibility emerges from the finding that the ground state of FPC features an unpaired electron on the carbene carbon. FPC could abstract a hydrogen atom from the N−H bond, as Scheme 3b depicts. An aniline radical (likely resonance-stabilized) and a new C−H bond would form. Next, a rebound process with the aniline radical would form the C−N bond and lead to the alkylated amine. (Fe−C homolytic bond cleavage, with a one-electron reduction of iron, would occur at the same time as, or before, this rebound step.) Indeed, Musaev and colleagues' computational results revealed that an iron nonheme carbene could abstract an H atom (in their case, from a C−H bond) with a reasonable barrier.[46]

Figure 6 presents the energy profile for each proposed pathway for singlet species (as Figure S26 presents, the triplet pathways had higher barriers). The lowest-energy transition state is for nucleophilic attack on the OSS surface (^{1OS}TS-NA), and it is very close in energy to the CSS nucleophilic attack transition state (^{1CS}TS-NA). The OSS H atom transfer (HAT) transition state is 6.5 kcal/mol higher in Gibbs free energy than ^{1OS}TS-NA. These results reveal N−H insertion will exclusively follow the nucleophilic attack pathway. The close-to-neutral NBO charge on the carbene carbon in the OSS FPC (see Figure 1) supports the claim the carbene can be electrophilic

DOI: 10.1021/jacs.6b04636
J. Am. Chem. Soc. 2016, 138, 9597−9610

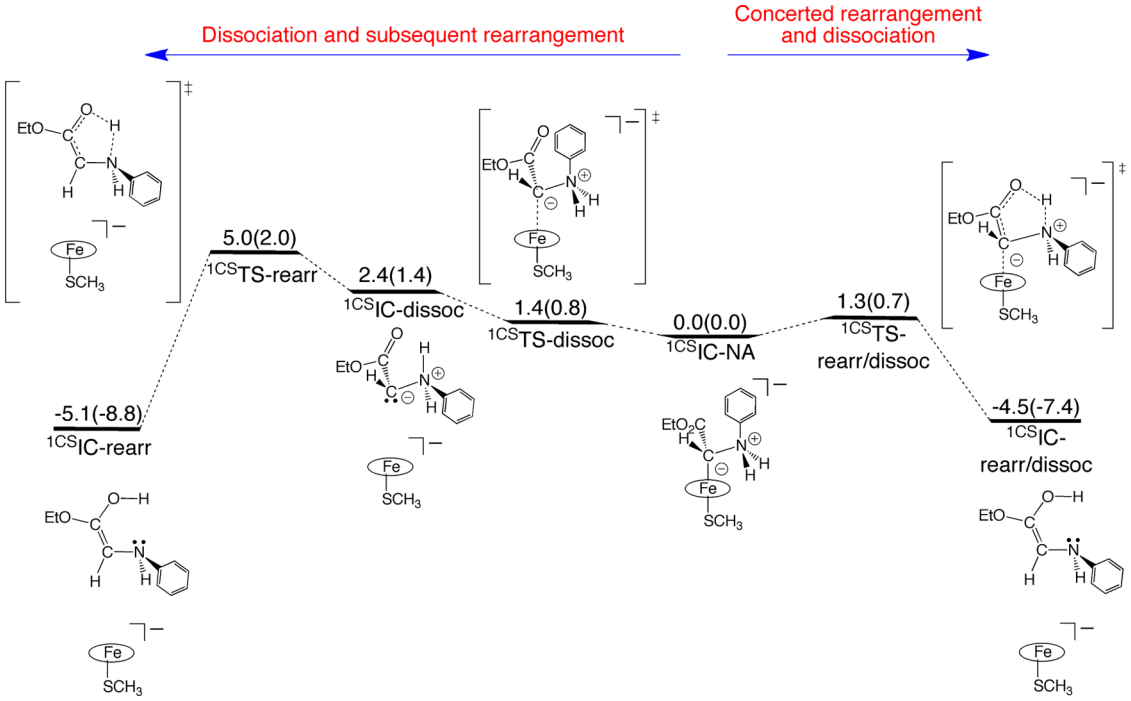

Figure 7. Energy profile for concerted rearrangement and dissociation of the iron-bound ylide (right) and for dissociation of the ylide followed by rearrangement (left) on the closed-shell singlet surface. Energies were computed at the B2//B1 level, and they are presented as relative electronic energy with zero-point correction outside of the parentheses and then relative Gibbs free energy inside the parentheses. Structures were optimized in chlorobenzene (SMD model). All values are dispersion-corrected. Note that this profile is plotted with respect to the electronic energies with zero-point correction.

within the negatively charged iron porphyrin carbene complex and thus bolsters the claim of this pathway's operating. Following the IRC of ^{1OS}TS-NA led to a closed-shell ylide intermediate (Figure S29) very much similar to that obtained from the IRC of ^{1CS}TS-NA.

Experimental studies on different substrates tend to also support the claim that nucleophilic attack occurs. Arnold, Fasan, and colleagues discovered the yield of N−H insertion product was quite sensitive to the steric bulk of substituents on the phenyl ring, even when electronic factors did not vary significantly across substituents.[28,29] The nucleophilic attack pathway should be quite sensitive to these effects, given the increase in steric crowding in the transition state and motion of the amine needed to achieve this close approach in the transition state. In contrast, for HAT, the motion of a hydrogen atom would require less displacement of the amine. Such sensitivity to steric bulk would be more difficult to rationalize if the mechanism involved HAT. Fasan noted myoglobin carbene-mediated S−H insertion exhibits nonlinear Hammett behavior and advanced a similar argument.[30] Arnold's observing only the single N−H insertion product from the enzyme supports the claim that steric bulk, which would be important in nucleophilic attack, influences the mechanism.[28]

If N−H insertion occurs by nucleophilic attack, what are the ramifications for substrate scope? Thus, far, only aromatic amines have been reported to undergo N−H insertion in enzymes.[28,29] In model systems, aliphatic amines have been reported to undergo N−H insertion.[15,16,18−20] However, myoglobin, with two mutations, mediated carbene S−H insertion with aliphatic thiols.[30] Aliphatic amines are protonated at neutral pH, and the active site would have to enable the amine to exist in a neutral, not protonated, form for nucleophilic attack to occur. Perhaps current systems' active sites are not sufficiently basic, so aliphatic amines are protonated and cannot act as nucleophiles. In an enzyme where an aliphatic amine exists in its neutral form, nucleophilic attack should be facile: aliphatic amines should be more nucleophilic than aromatic ones. This work's findings reveal an appropriately designed enzyme may catalyze aliphatic N−H insertion (via nucleophilic attack), expanding the substrate scope beyond what has been experimentally reported in enzymes.

Looking at the carbene formation and nucleophilic attack reaction sequence enables understanding substrate effects. When experimentalists used $C(CH_3)(CO_2Et)(N_2)$ and $CH(CONEt_2)(N_2)$ diazo reagents, the yields of N−H and S−H insertion products decreased drastically.[28,30] With these modifications, the diazo derivative would be less electrophilic and less likely to accept an electron from iron to form the RC-EDA_{close} species. This RC is crucial because it enables the system to access the OSS spin surface, on which the barrier for N_2 loss is the lowest. In addition, the resulting carbenes would be more sterically crowded, which could render nucleophilic attack more difficult.

3.2. Subsequent Ylide Transformations. Nucleophilic attack produces an ylide that is weakly bound to iron, with an Fe−C distance of 2.21 Å. This section will first explore ylide reactivity and then comment on these findings with regards to enantioselectivity and substrate scope. Figure 7 presents two possible subsequent reactions to form the final product. One, on the right-hand side, involves ylide rearrangement, with proton transfer through a five-membered ring, to form an enol. The potential energy scan and IRC calculation involving this transition state showed Fe−C elongation accompanies O−H bond formation (Figures S33 and S34). Upon optimization, $^{1CS}IC_{rearr/dissoc}$ had an Fe−C distance of 3.74 Å. Thus, this

DOI: 10.1021/jacs.6b04636
J. Am. Chem. Soc. 2016, 138, 9597−9610

transition state represents both rearrangement and dissociation in a concerted process. The second process, on the left-hand side of Figure 7, commences with ylide dissociation from the iron porphyrin. Then, the free ylide rearranges through a five-membered transition state to form an enol. The dissociation transition state is lower in energy than the dissociation product due to the stabilizing elongation in the Fe−C distance from the transition state to the product: also, in the dissociated ylide, the carbonyl group adjacent to the negatively charged carbon enables delocalization of the negative charge. Similar internal proton transfers have been reported for another metal carbene system.[113]

The first pathway, with simultaneous rearrangement and dissociation, has a lower overall energy barrier and thus is most likely to occur. This reaction is already exergonic, and once the Fe−C bond is broken, the iron porphyrin can also relax electronically to the quintet state, rendering the reactions even more favorable, as Figure S35 presents. A potential energy scan to evaluate the possibility of direct proton transfer from nitrogen to carbon (a three-membered transition state) gave rise to a large estimated electronic energy barrier of 60.0 kcal/mol (see Figure S36): this process was deemed infeasible. The enol should tautomerize to the ketone easily. An acidic or basic residue in the enzyme, or a water molecule, could facilitate the transformation. This five-membered ring transition state articulates the precise process by which the ylide becomes the final product in further detail than has been reported before.[14,16,17,30]

This finding suggests the rearrangement is not inherently enantioselective. The current work found that enol formation will occur either after dissociation or simultaneously with the dissociation event: either way, a free enol will result. The molecule does not have stereocenters, so rearrangement should not exhibit a stereochemical preference in an environment lacking chirality. In a model system for N−H insertion with a postulated ylide intermediate, enantioselectivity was not observed,[16] but enantioselectivity was reported in S−H insertion and N−H insertion with artificial metalloenzymes.[30,114] The present findings cannot explain enantioselectivity and thus suggest the protein exerts a special effect to impart stereochemical preferences, as was previously speculated and rationalized.[30] Indeed, different myoglobin mutants exhibited dramatically different enantiomeric excess values for carbene insertion into the S−H bond, showing the protein's role.[30]

In addition to enantioselectivity, one can also consider possible consequences of this finding for substrate scope. In Arnold and Fasan's N−H and S−H insertion work, the carbene carbon always has an α-carbonyl group (Scheme 4a).[28−30] The prevalence of this α-carbonyl group is striking in light of findings that an iron porphyrin diphenyl carbene has been synthesized in a model system,[7] and in light of computational results that diazo reagents besides $CH(CO_2Et)(N_2)$ can react with iron porphyrins to form iron porphyrin carbenes.[56] Scheme 4b shows that, while a carbene with an α-carbonyl group offers an opportunity for the corresponding ylide to rearrange via a five-membered transition state, such a pathway is not available for diphenyl carbenes. If they form an ylide, that ylide could only rearrange through a three-membered transition state (assuming there is no external species assisting with proton transfer).

3.3. Comments on HAT. The previous sections found N−H insertion occurs by nucleophilic attack and subsequent ylide

Scheme 4. (a) A Diazo Reagent with an α-Carbonyl Group Observed in the Work of Arnold, Fasan, and Colleagues (Left) and a Reagent with Diphenyl Substituents Not Yet Employed in Artificial Metalloenzyme Work (Right); (b) The Putative Five-Membered Transition State (Left) and Three-Membered Transition State (Right) for Rearrangement of the Corresponding Carbene-Derived Ylides

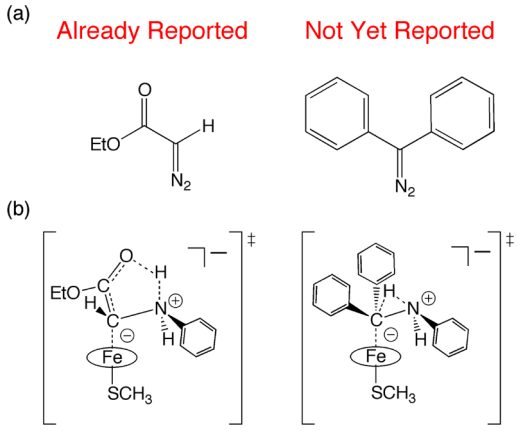

rearrangement. Although it does not occur in the present system, understanding the HAT pathway is also worthwhile in order to compare oxo and carbene reactivity and comprehend potential ramifications for other carbene-mediated reactions. Figure S30 presents the SNOs for the H-abstraction reaction transition state. One SNO involves both the N−H bond and the carbene, in an arrangement which is the signature of a hydrogen atom transfer (HAT) process.[115] In studies of H-abstraction mediated by iron-oxo complexes, proton-coupled electron transfer (PCET) and HAT have both been reported.[115] Efforts to locate a PCET transition state did not succeed in the present work.

Why can iron-oxo complexes react by HAT or PCET, while it appears the carbene can only accomplish HAT? The carbene has one nonbonding electron. Thus, aniline's proton and electron must migrate to the same orbital in order to form the C−H bond. HAT must occur, and PCET is not possible. In contrast, the oxo ligand has multiple nonbonding electrons,[116,117] so it can provide one or both of the electrons in the forming O−H bond: the entering electron can migrate to the same orbital as the proton or to a different orbital. HAT and PCET are both feasible: with several unpaired electrons, iron oxo species can abstract hydrogen atoms in different ways.[115,118,119] The carbene and oxo complexes' different electronic structures give rise to different reactivity possibilities.

This finding that carbenes can abstract an H atom from an N−H bond, which has a decently high bond dissociation energy,[120] with a reasonable barrier suggests that carbenes can perhaps accomplish HAT from some C−H bonds. Indeed, Musaev and colleagues found an iron nonheme carbene abstracted an H atom from a C−H bond with a moderate barrier.[46] Without lone pairs, C atoms cannot react with the carbene via nucleophilic attack, so HAT is the only C−H insertion pathway accessible.

After HAT, alkyl radical rebound would very likely occur, so the reaction would culminate in C−C coupling. Indeed, Arnold and colleagues' recent patent includes preliminary claims concerning such a process.[114] The only mechanistic work (to the best of our knowledge) on iron porphyrin carbene-

DOI: 10.1021/jacs.6b04636
J. Am. Chem. Soc. 2016, 138, 9597−9610

mediated C−H insertion involves a more oxidized iron porphyrin carbene and suggests a concerted process, which should have a high entropic penalty.[21] The current work considers iron in the same oxidation state as in Arnold's system and suggests a more entropically plausible mechanistic possibility. Currently, chemists often employ toxic and costly palladium catalysts for this crucial coupling reaction.[121−123] Efforts to develop alternative catalysts are underway,[123,124] and iron porphyrins and P450s constitute nontoxic, low-cost candidates. Furthermore, considering different reactivity possibilities, the discovery of this open-shell singlet ground state suggests iron porphyrin carbenes may be able to undergo a range of reactions previously reported for cobalt complexes which also have carbene-based radicals.[125,126]

Considering the N−H insertion reactivity landscape both enables understanding why the ylide resulting from nucleophilic attack on the diphenyl carbene may not be able to react further and suggests a possible alternate pathway. The ylide may not react further due to the three-membered ring transition state's being high in energy (no internal base is available, so there is no five-membered ring option). However, an internal base in the carbene would not be necessary for HAT. Thus, in an enzyme or other system designed so HAT from the N−H bond can occur, a diphenyl carbene (and any other carbene without an internal base) may be able to mediate N−H insertion processes. Enabling these different carbenes to react would amplify this reaction's synthetic potential.

CONCLUSIONS

This work explored the new frontier of iron porphyrin carbenes, articulating novel insights into their electronic structure, formation, and reactivity. Such findings are valuable for three reasons. First, they prompt comparisons to iron-superoxo and oxo species, particularly intriguing in light of our group's long-standing interest in these fields.[59,127] We can interpret these carbenes within the landscape of iron-superoxo and oxo compounds that we have been involved in mapping. Second, these discoveries enable understanding experimentally observed phenomena, such as different species' relative reactivities. Third, these findings both suggest ways to think about engineering systems with higher yields and a wider substrate scope and suggest possible causes of enantioselectivity. In the future, understanding the enzyme environment's effect with quantum mechanical/molecular mechanical techniques is of interest. This work's key findings are as follows:

(a) The ground electronic state of the terminal FPC is an open-shell singlet. SNOs reveal an unpaired electron on the carbene carbon is antiferromagnetically coupled to an unpaired electron on the iron, highly analogous to the bonding in and electronic structure of ferric superoxide complexes.[61−63] This finding stands in contrast to previous reports of closed-shell singlet iron porphyrin carbenes.[53,56] The carbonyl group adjacent to the carbene carbon stabilizes this electronic configuration, and we speculate tuning the carbene's substituents may alter the ground electronic state of an iron porphyrin carbene.

(b) N_2 loss from EDA to form the iron porphyrin carbene has the lowest barrier on the OSS surface. SNOs highlight that, in the OSS RC and transition state, iron donates electron density to EDA, populating a C−N antibonding orbital. This electronic factor, contributing to cleaving the C−N bond, helps to explain why the OSS transition state is significantly lower in energy than the previously reported CSS transition state.[56] Experimentally, the yield decreased with more electron-rich diazo derivatives.[28,30] In this situation, the crucial electron transfer from iron to the diazo species would be more difficult. Electron donation from iron to form the active species in the carbene system is reminiscent of the iron-oxo active species formation pathway in P450s.[59,112]

(c) The iron porphyrin carbene's N−H insertion reaction follows a nucleophilic attack pathway, forming an ylide. This finding suggests the reaction should be sensitive to sterics and thus agrees with experimental reports suggesting factors other than electronic ones influence reactivity.[28,30] Thus, this discovery suggests that, in an appropriately constructed metalloenzyme, aliphatic amines should be able to undergo N−H insertion, as was reported in model systems.[15,16,18−20]

(d) The ylide formed by nucleophilic attack undergoes simultaneous rearrangement and dissociation from iron. The rearrangement proceeds via a five-membered proton transfer transition state to form an enol, which should be able to facilely tautomerize to the final alkylated amine product. This discovery does not indicate an intrinsically enantioselective process and confirms suggestions that the enzyme's architecture is crucial for achieving enantioselectivity.[30] Designing such systems represents an avenue for further experimental work. Indeed, recent studies expanded the repertoire of engineered P450s.[128,129] The five-membered transition state requires an internal base and may help explain the prevalence of an α-carbonyl group in carbene studies.[28−30]

(e) The H-abstraction barrier is higher than the nucleophilic attack barrier but is still reasonably low. H-abstraction transition state SNOs revealed a HAT process operates.[115] Unlike iron-oxo complexes,[115] iron porphyrin carbenes appear incapable of PCET, due to their different electronic structure.

This work employs computational techniques as keys to unlock trailblazing insights into iron porphyrin carbenes' electronic structure, formation, and reactivity. These discoveries prompt enriching comparisons with iron-superoxo and oxo species. Furthermore, they give rise to a fertile range of explanations for experimental phenomena and predictions for future work, which both experimentalists and computationalists can harvest in order to further expand these systems' flourishing potential.

ASSOCIATED CONTENT

Supporting Information

The Supporting Information is available free of charge on the ACS Publications website at DOI: 10.1021/jacs.6b04636.

Yamaguchi correction data, SH ligand data, additional orbitals, and geometric and energetic data, as well as absolute energies and Cartesian coordinates of species in the main text (PDF)

AUTHOR INFORMATION

Corresponding Author

*E-mail: sason@yfaat.ch.huji.ac.il.

Notes

The authors declare no competing financial interest.

DOI: 10.1021/jacs.6b04636
J. Am. Chem. Soc. 2016, 138, 9597−9610

■ ACKNOWLEDGMENTS

The authors thank Dr. David Danovich for helpful discussions on electronic structure. D.A.S. thanks the United States−Israel Educational Foundation and the Fulbright U.S. Student Program for her fellowship. D.M. and B.W. thank the Planning and Budgeting Committee of The Council for Higher Education in Israel for their fellowships. S.S. thanks the Israel Science Foundation (ISF 1183/13) for support of the work.

■ REFERENCES

(1) Gillingham, D.; Fei, N. *Chem. Soc. Rev.* **2013**, *42*, 4918.
(2) Doyle, M. P.; Duffy, R.; Ratnikov, M.; Zhou, L. *Chem. Rev.* **2010**, *110*, 704.
(3) Davies, H. M. L.; Gregg, T. M. *Tetrahedron Lett.* **2002**, *43*, 4951.
(4) Zhang, W.-B.; Lin, G.; Shao, W.-B.; Gong, J.-X.; Yang, Z. *Chem. - Asian J.* **2015**, *10*, 903.
(5) Gong, J.; Lin, G.; Sun, W.; Li, C.-C.; Yang, Z. *J. Am. Chem. Soc.* **2010**, *132*, 16745.
(6) Mansuy, D.; Lange, M.; Chottard, J. C.; Bartoli, J. F.; Chevrier, B.; Weiss, R. *Angew. Chem., Int. Ed. Engl.* **1978**, *17*, 781.
(7) Li, Y.; Huang, J.-S.; Zhou, Z.-Y.; Che, C.-M.; You, X.-Z. *J. Am. Chem. Soc.* **2002**, *124*, 13185.
(8) Guerin, P.; Battioni, J.-P.; Chottard, J.-C.; Mansuy, D. *J. Organomet. Chem.* **1981**, *218*, 201.
(9) Artaud, I.; Gregoire, N.; Leduc, P.; Mansuy, D. *J. Am. Chem. Soc.* **1990**, *112*, 6899.
(10) Artaud, I.; Gregoire, N.; Battioni, J.-P.; Dupre, D.; Mansuy, D. *J. Am. Chem. Soc.* **1988**, *110*, 8714.
(11) Lange, M.; Battioni, J. P.; Mansuy, D. *J. Chem. Soc., Chem. Commun.* **1981**, 888.
(12) Cheng, G.; Mirafzal, G. A.; Woo, L. K. *Organometallics* **2003**, *22*, 1468.
(13) Nicolas, I.; Le Maux, P.; Simonneaux, G. *Tetrahedron Lett.* **2008**, *49*, 5793.
(14) Baumann, L. K.; Mbuvi, H. M.; Du, G.; Woo, L. K. *Organometallics* **2007**, *26*, 3995.
(15) Aviv, I.; Gross, Z. *Synlett* **2006**, 951.
(16) Aviv, I.; Gross, Z. *Chem. - Eur. J.* **2008**, *14*, 3995.
(17) Xu, X.; Li, C.; Tao, Z.; Pan, Y. *Adv. Synth. Catal.* **2015**, *357*, 3341.
(18) Srour, H. F.; Le Maux, P.; Chevance, S.; Carrié, D.; Le Yondre, N.; Simonneaux, G. *J. Mol. Catal. A: Chem.* **2015**, *407*, 194.
(19) Aviv, I.; Gross, Z. *Chem. Commun.* **2006**, 4477.
(20) Ma, C.; Xing, D.; Zhai, C.; Che, J.; Liu, S.; Wang, J.; Hu, W. *Org. Lett.* **2013**, *15*, 6140.
(21) Mbuvi, H. M.; Woo, L. K. *Organometallics* **2008**, *27*, 637.
(22) Chen, Y.; Huang, L.; Ranade, M. A.; Zhang, X. P. *J. Org. Chem.* **2003**, *68*, 3714.
(23) Mbuvi, H. M.; Klobukowski, E. R.; Roberts, G. M.; Woo, L. K. *J. Porphyrins Phthalocyanines* **2010**, *14*, 284.
(24) Correia, M. A.; Ortiz de Montellano, P. R. In *Cytochrome P450: Structure, Mechanism, and Biochemistry*; Ortiz de Montellano, P. R., Ed.; Kluwer Academic/Plenum Publishers: New York, 2005; pp 247−322.
(25) Coelho, P. S.; Brustad, E. M.; Kannan, A.; Arnold, F. H. *Science* **2013**, *339*, 307.
(26) Coelho, P. S.; Wang, Z. J.; Ener, M. E.; Baril, S. A.; Kannan, A.; Arnold, F. H.; Brustad, E. M. *Nat. Chem. Biol.* **2013**, *9*, 485.
(27) Bordeaux, M.; Tyagi, V.; Fasan, R. *Angew. Chem.* **2015**, *127*, 1764.
(28) Wang, Z. J.; Peck, N. E.; Renata, H.; Arnold, F. H. *Chem. Sci.* **2014**, *5*, 598.
(29) Sreenilayam, G.; Fasan, R. *Chem. Commun.* **2015**, *51*, 1532.
(30) Tyagi, V.; Bonn, R. B.; Fasan, R. *Chem. Sci.* **2015**, *6*, 2488.
(31) Tyagi, V.; Fasan, R. *Angew. Chem., Int. Ed.* **2016**, *55*, 2512.
(32) Weissenborn, M. J.; Löw, S. A.; Borlinghaus, N.; Kuhn, M.; Kummer, S.; Rami, F.; Plietker, B.; Hauer, B. *ChemCatChem* **2016**, *8*, 1636.
(33) Bos, J.; Roelfes, G. *Curr. Opin. Chem. Biol.* **2014**, *19*, 135.
(34) Pàmies, O.; Diéguez, M.; Bäckvall, J.-E. *Adv. Synth. Catal.* **2015**, *357*, 1567.
(35) Lewis, J. C. *ACS Catal.* **2013**, *3*, 2954.
(36) Ilie, A.; Reetz, M. T. *Isr. J. Chem.* **2015**, *55*, 51.
(37) Sun, Z.; Lonsdale, R.; Kong, X.-D.; Xu, J.-H.; Zhou, J.; Reetz, M. T. *Angew. Chem., Int. Ed.* **2015**, *54*, 12410.
(38) Renata, H.; Wang, Z. J.; Arnold, F. H. *Angew. Chem., Int. Ed.* **2015**, *54*, 3351.
(39) Agudo, R.; Roiban, G.-D.; Lonsdale, R.; Ilie, A.; Reetz, M. T. *J. Org. Chem.* **2015**, *80*, 950.
(40) Gober, J. G.; Rydeen, A. E.; Gibson-O'Grady, E. J.; Leuthaeuser, J. B.; Fetrow, J. S.; Brustad, E. M. *ChemBioChem* **2016**, *17*, 394.
(41) Roughley, S. D.; Jordan, A. M. *J. Med. Chem.* **2011**, *54*, 3451.
(42) Zheng, S.; Luo, X.; Chen, G.; Zhu, W.; Shen, J.; Chen, K.; Jiang, H. *J. Chem. Inf. Model.* **2005**, *45*, 856.
(43) Bariwal, J.; Van der Eycken, E. *Chem. Soc. Rev.* **2013**, *42*, 9283.
(44) Jennings, G. K.; Ritchie, C. M.; Shock, L. S.; Lyons, C. E.; Hackett, J. C. *Mol. Pharmacol.* **2016**, *90*, 42.
(45) Wolf, C. R.; Mansuy, D.; Nastainczyk, W.; Deutschmann, G.; Ullrich, V. *Mol. Pharmacol.* **1977**, *13*, 698.
(46) Varela-Álvarez, A.; Musaev, D. G. *Chem. Sci.* **2013**, *4*, 3758.
(47) Tatsumi, K.; Hoffmann, R. *Inorg. Chem.* **1981**, *20*, 3771.
(48) Schöneboom, J. C.; Lin, H.; Reuter, N.; Thiel, W.; Cohen, S.; Ogliaro, F.; Shaik, S. *J. Am. Chem. Soc.* **2002**, *124*, 8142.
(49) Ogliaro, F.; Harris, N.; Cohen, S.; Filatov, M.; de Visser, S. P.; Shaik, S. *J. Am. Chem. Soc.* **2000**, *122*, 8977.
(50) de Visser, S. P.; Ogliaro, F.; Harris, N.; Shaik, S. *J. Am. Chem. Soc.* **2001**, *123*, 3037.
(51) Ogliaro, F.; de Visser, S. P.; Groves, J. T.; Shaik, S. *Angew. Chem.* **2001**, *113*, 2958.
(52) Taxak, N.; Patel, B.; Bharatam, P. V. *Inorg. Chem.* **2013**, *52*, 5097.
(53) Khade, R. L.; Fan, W.; Ling, Y.; Yang, L.; Oldfield, E.; Zhang, Y. *Angew. Chem., Int. Ed.* **2014**, *53*, 7574.
(54) Che, C.-M.; Zhou, C.-Y.; Wong, E. L.-M. In *Iron Catalysis*; Plietker, B., Ed.; Topics in Organometallic Chemistry; Springer-Verlag Berlin Heidelberg: Berlin, 2011; Vol. 33, pp 111−138.
(55) Russell, S. K.; Hoyt, J. M.; Bart, S. C.; Milsmann, C.; Stieber, S. C. E.; Semproni, S. P.; DeBeer, S.; Chirik, P. J. *Chem. Sci.* **2014**, *5*, 1168.
(56) Khade, R. L.; Zhang, Y. *J. Am. Chem. Soc.* **2015**, *137*, 7560.
(57) Wang, F.; Meng, Q.; Li, M. *Int. J. Quantum Chem.* **2008**, *108*, 945.
(58) Fallah, H.; Horng, F.; Cundari, T. R. *Organometallics* **2016**, *35*, 950.
(59) Shaik, S.; Cohen, S.; Wang, Y.; Chen, H.; Kumar, D.; Thiel, W. *Chem. Rev.* **2010**, *110*, 949.
(60) Shaik, S.; Kumar, D.; de Visser, S. P.; Altun, A.; Thiel, W. *Chem. Rev.* **2005**, *105*, 2279.
(61) Chen, H.; Ikeda-Saito, M.; Shaik, S. *J. Am. Chem. Soc.* **2008**, *130*, 14778.
(62) Rovira, C.; Kunc, K.; Hutter, J.; Ballone, P.; Parrinello, M. *J. Phys. Chem. A* **1997**, *101*, 8914.
(63) Jensen, K. P.; Roos, B. O.; Ryde, U. *J. Inorg. Biochem.* **2005**, *99*, 45.
(64) Frisch, M. J.; Trucks, G. W.; Schlegel, H. B.; Scuseria, G. E.; Robb, M. A.; Cheeseman, J. R.; Scalmani, G.; Barone, V.; Mennucci, B.; Petersson, G. A.; Nakatsuji, H.; Caricato, M.; Li, X.; Hratchian, H. P.; Izmaylov, A. F.; Bloino, J.; Zheng, G.; Sonnenberg, J. L.; Hada, M.; Ehara, M.; Toyota, K.; Fukuda, R.; Hasegawa, J.; Ishida, M.; Nakajima, T.; Honda, Y.; Kitao, O.; Nakai, H.; Vreven, T.; Montgomery, J. A., Jr.; Peralta, J. E.; Ogliaro, F.; Bearpark, M.; Heyd, J. J.; Brothers, E.; Kudin, K. N.; Staroverov, V. N.; Keith, T.; Kobayashi, R.; Normand, J.; Raghavachari, K.; Rendell, A.; Burant, J. C.; Iyengar, S. S.; Tomasi, J.; Cossi, M.; Rega, N.; Millam, J. M.; Klene, M.; Knox, J. E.; Cross, J. B.; Bakken, V.; Adamo, C.; Jaramillo, J.; Gomperts, R.; Stratmann, R. E.; Yazyev, O.; Austin, A. J.; Cammi, R.; Pomelli, C.; Ochterski, J. W.; Martin, R. L.; Morokuma, K.; Zakrzewski, V. G.; Voth, G. A.; Salvador, P.; Dannenberg, J. J.; Dapprich, S.; Daniels, A. D.; Farkas, O.;

DOI: 10.1021/jacs.6b04636
J. Am. Chem. Soc. 2016, 138, 9597−9610

Foresman, J. B.; Ortiz, J. V.; Cioslowski, J.; Fox, D. J. *Gaussian 09*, Revision D.01; Gaussian, Inc.: Wallingford, CT, 2013.
(65) Becke, A. D. *J. Chem. Phys.* **1992**, *96*, 2155.
(66) Becke, A. D. *J. Chem. Phys.* **1992**, *97*, 9173.
(67) Becke, A. D. *J. Chem. Phys.* **1993**, *98*, 5648.
(68) Lee, C.; Yang, W.; Parr, R. G. *Phys. Rev. B: Condens. Matter Mater. Phys.* **1988**, *37*, 785.
(69) Hay, P. J.; Wadt, W. R. *J. Chem. Phys.* **1985**, *82*, 270.
(70) Wadt, W. R.; Hay, P. J. *J. Chem. Phys.* **1985**, *82*, 284.
(71) Hay, P. J.; Wadt, W. R. *J. Chem. Phys.* **1985**, *82*, 299.
(72) Hehre, W. J.; Ditchfield, R.; Pople, J. A. *J. Chem. Phys.* **1972**, *56*, 2257.
(73) Clark, T.; Chandrasekhar, J.; Spitznagel, G. W.; Schleyer, P. V. R. *J. Comput. Chem.* **1983**, *4*, 294.
(74) Francl, M. M.; Pietro, W. J.; Hehre, W. J.; Binkley, J. S.; Gordon, M. S.; DeFrees, D. J.; Pople, J. A. *J. Chem. Phys.* **1982**, *77*, 3654.
(75) Frisch, M. J.; Pople, J. A.; Binkley, J. S. *J. Chem. Phys.* **1984**, *80*, 3265.
(76) Marenich, A. V.; Cramer, C. J.; Truhlar, D. G. *J. Phys. Chem. B* **2009**, *113*, 6378.
(77) Usharani, D.; Janardanan, D.; Shaik, S. *J. Am. Chem. Soc.* **2011**, *133*, 176.
(78) Li, C.; Wu, W.; Cho, K.-B.; Shaik, S. *Chem. - Eur. J.* **2009**, *15*, 8492.
(79) Weigend, F.; Ahlrichs, R. *Phys. Chem. Chem. Phys.* **2005**, *7*, 3297.
(80) Weigend, F. *Phys. Chem. Chem. Phys.* **2006**, *8*, 1057.
(81) Grimme, S.; Ehrlich, S.; Goerigk, L. *J. Comput. Chem.* **2011**, *32*, 1456.
(82) Reed, A. E.; Weinstock, R. B.; Weinhold, F. *J. Chem. Phys.* **1985**, *83*, 735.
(83) Chen, H.; Lai, W.; Shaik, S. *J. Phys. Chem. Lett.* **2010**, *1*, 1533.
(84) Altun, A.; Breidung, J.; Neese, F.; Thiel, W. *J. Chem. Theory Comput.* **2014**, *10*, 3807.
(85) Wang, B.; Li, C.; Cho, K.-B.; Nam, W.; Shaik, S. *J. Chem. Theory Comput.* **2013**, *9*, 2519.
(86) Zhao, Y.; Truhlar, D. G. *J. Chem. Phys.* **2006**, *125*, 194101.
(87) Tao, J.; Perdew, J. P.; Staroverov, V. N.; Scuseria, G. E. *Phys. Rev. Lett.* **2003**, *91*, 146401.
(88) Zhao, Y.; Truhlar, D. G. *Theor. Chem. Acc.* **2008**, *120*, 215.
(89) Boese, A. D.; Martin, J. M. L. *J. Chem. Phys.* **2004**, *121*, 3405.
(90) Seeger, R.; Pople, J. A. *J. Chem. Phys.* **1977**, *66*, 3045.
(91) Bauernschmitt, R.; Ahlrichs, R. *J. Chem. Phys.* **1996**, *104*, 9047.
(92) Schlegel, H. B.; McDouall, J. J. W. In *Computational Advances in Organic Chemistry: Molecular Structure and Reactivity (NATO ASI Series, Vol. 330)*; Ögretir, C., Csizmadia, I. G., Eds.; Springer: The Netherlands, 1991; pp 167−185.
(93) Gräfenstein, J.; Kraka, E.; Cremer, D. *Chem. Phys. Lett.* **1998**, *288*, 593.
(94) Gräfenstein, J.; Kraka, E.; Filatov, M.; Cremer, D. *Int. J. Mol. Sci.* **2002**, *3*, 360.
(95) Abe, M. *Chem. Rev.* **2013**, *113*, 7011.
(96) Abe, M.; Ye, J.; Mishima, M. *Chem. Soc. Rev.* **2012**, *41*, 3808.
(97) Schreiner, P. R.; Navarro-Vázquez, A.; Prall, M. *Acc. Chem. Res.* **2005**, *38*, 29.
(98) Yamanaka, S.; Takeda, R.; Shoji, M.; Kitagawa, Y.; Honda, H.; Yamaguchi, K. *Int. J. Quantum Chem.* **2005**, *105*, 605.
(99) Kitagawa, Y.; Saito, T.; Ito, M.; Shoji, M.; Koizumi, K.; Yamanaka, S.; Kawakami, T.; Okumura, M.; Yamaguchi, K. *Chem. Phys. Lett.* **2007**, *442*, 445.
(100) Lonsdale, R.; Harvey, J. N.; Mulholland, A. J. *J. Phys. Chem. Lett.* **2010**, *1*, 3232.
(101) Dzik, W. I.; Xu, X.; Zhang, X. P.; Reek, J. N. H.; de Bruin, B. *J. Am. Chem. Soc.* **2010**, *132*, 10891.
(102) Dzik, W. I.; Reek, J. N. H.; de Bruin, B. *Chem. - Eur. J.* **2008**, *14*, 7594.
(103) Weiss, J. J. *Nature* **1964**, *202*, 83.
(104) Bellow, J. A.; Stoian, S. A.; van Tol, J.; Ozarowski, A.; Lord, R. L.; Groysman, S. *J. Am. Chem. Soc.* **2016**, *138*, 5531.
(105) Belof, J. L.; Cioce, C. R.; Xu, X.; Zhang, X. P.; Space, B.; Woodcock, H. L. *Organometallics* **2011**, *30*, 2739.
(106) Lu, H.; Dzik, W. I.; Xu, X.; Wojtas, L.; de Bruin, B.; Zhang, X. P. *J. Am. Chem. Soc.* **2011**, *133*, 8518.
(107) Aldajaei, J. T.; Gronert, S. *Int. J. Mass Spectrom.* **2012**, *316-318*, 68.
(108) Dzik, W. I.; Zhang, X. P.; de Bruin, B. *Inorg. Chem.* **2011**, *50*, 9896.
(109) Comanescu, C. C.; Vyushkova, M.; Iluc, V. M. *Chem. Sci.* **2015**, *6*, 4570.
(110) Li, F.; Xiao, L.; Li, Y.; Chen, C.; Liu, L. *Chem. Commun.* **2015**, *51*, 11964.
(111) Li, F.; Xiao, L.; Liu, L. *Sci. Rep.* **2016**, *6*, 22876.
(112) Groves, J. T. In *Cytochrome P450: Structure, Mechanism, and Biochemistry*; Ortiz de Montellano, P. R., Ed.; Kluwer Academic/Plenum Publishers: New York, 2005; pp 1−44.
(113) Liu, Y.; Yu, Z.; Luo, Z.; Zhang, J. Z.; Liu, L.; Xia, F. *J. Phys. Chem. A* **2016**, *120*, 1925.
(114) Coelho, P.; Arnold, F. H.; Lewis, J. C.; Wang, Z. *In Vivo and In Vitro Carbene Insertion and Nitrene Transfer Reactions Catalyzed by Heme Enzymes*. 14/676744, 2015.
(115) Usharani, D.; Lacy, D. C.; Borovik, A. S.; Shaik, S. *J. Am. Chem. Soc.* **2013**, *135*, 17090.
(116) Shaik, S.; Lai, W.; Chen, H.; Wang, Y. *Acc. Chem. Res.* **2010**, *43*, 1154.
(117) Usharani, D.; Lai, W.; Li, C.; Chen, H.; Danovich, D.; Shaik, S. *Chem. Soc. Rev.* **2014**, *43*, 4968.
(118) Boaz, N. C.; Bell, S. R.; Groves, J. T. *J. Am. Chem. Soc.* **2015**, *137*, 2875.
(119) Usharani, D.; Janardanan, D.; Li, C.; Shaik, S. *Acc. Chem. Res.* **2013**, *46*, 471.
(120) Bordwell, F. G.; Zhang, X.-M.; Cheng, J.-P. *J. Org. Chem.* **1993**, *58*, 6410.
(121) Johansson Seechurn, C. C. C.; Kitching, M. O.; Colacot, T. J.; Snieckus, V. *Angew. Chem., Int. Ed.* **2012**, *51*, 5062.
(122) Miyaura, N.; Suzuki, A. *Chem. Rev.* **1995**, *95*, 2457.
(123) Corbet, J.-P.; Mignani, G. *Chem. Rev.* **2006**, *106*, 2651.
(124) Sherry, B. D.; Fürstner, A. *Acc. Chem. Res.* **2008**, *41*, 1500.
(125) Paul, N. D.; Mandal, S.; Otte, M.; Cui, X.; Zhang, X. P.; de Bruin, B. *J. Am. Chem. Soc.* **2014**, *136*, 1090.
(126) Paul, N. D.; Chirila, A.; Lu, H.; Zhang, X. P.; de Bruin, B. *Chem. - Eur. J.* **2013**, *19*, 12953.
(127) Shaik, S.; Chen, H.; Janardanan, D. *Nat. Chem.* **2011**, *3*, 19.
(128) McIntosh, J. A.; Farwell, C. C.; Arnold, F. H. *Curr. Opin. Chem. Biol.* **2014**, *19*, 126.
(129) McIntosh, J. A.; Heel, T.; Buller, A. R.; Chio, L.; Arnold, F. H. *J. Am. Chem. Soc.* **2015**, *137*, 13861.

DOI: 10.1021/jacs.6b04636
J. Am. Chem. Soc. 2016, 138, 9597−9610